Dynamic Structural Effects on the Second-Harmonic Generation of Tryptophane-Rich Peptides and Gramicidin A

Seibert, Jakob; Champagne, Benoît; Grimme, Stefan; De Wergifosse, Marc

Published in:
The Journal of Physical Chemistry. B, Condensed matter, materials, surfaces, interfaces & biophysical

DOI:
10.1021/acs.jpcb.0c00643

Publication date:
2020

Document Version
Publisher's PDF, also known as Version of record

THE JOURNAL OF PHYSICAL CHEMISTRY B

pubs.acs.org/JPCB Article

Dynamic Structural Effects on the Second-Harmonic Generation of Tryptophane-Rich Peptides and Gramicidin A

Jakob Seibert, Benoît Champagne, Stefan Grimme,* and Marc de Wergifosse*

Cite This: J. Phys. Chem. B 2020, 124, 2568–2578 Read Online

ACCESS | Metrics & More | Article Recommendations | Supporting Information

ABSTRACT: Peptide chains can model endogenous biotags for applications in second-harmonic imaging microscopy. Such structures are flexible which may strongly affect their structure−property relationship. Here, we explore quantum-mechanically the conformational space of a set of tryptophan-rich model peptides. This has become feasible because of the recently proposed meta-dynamics method based on efficient tight-binding (TB) calculations. The TB version of the simplified time-dependent density functional theory (sTD-DFT-*x*TB) method is used to evaluate the first hyperpolarizability (β). These new tools enable us to calculate nonlinear optical properties for systems with several thousand atoms and/or to screen large structure ensembles. First, we show that the indole chromophore in tryptophan residues dominates the β response of these systems. Their relative orientation mostly determines the global β tensor and affects the static β response. The results underline the importance of finding low-energy conformers for modeling β of flexible molecules. Additionally, we compare calculated and extrapolated experimental static β. The sTD-DFT-*x*TB method is capable of providing reliable second-harmonic generation values for tryptophan-rich systems at a fraction of the computational cost of the commonly used TD-DFT/TD-HF levels of theory.

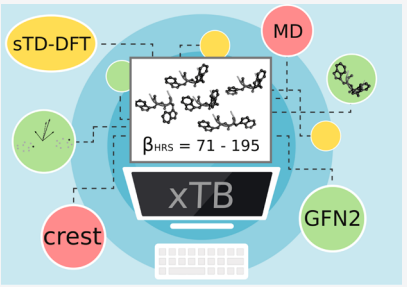

INTRODUCTION

Second harmonic imaging microscopy (SHIM)[1−4] has been developed for contrast enhancement of noncentrosymmetric molecular arrangements where the so-called second-harmonic generation (SHG) occurs. Information about the molecular organization of the chromophores can be extracted from SHG imaging data because the signal is polarization-dependent. SHIM is used as a high-resolution biological imaging technique where the SHG polarization anisotropy yields information about molecular orientation. Furthermore, it enables analyzing the degree of organization of proteins in tissues, related to their healthy or unhealthy state.[3] SHIM biotags could be endogenous such as ordered structures of collagen,[5−7] microtubule, or miosin.[1,3] Exogenous biotags on the other hand should be carefully applied to avoid phototoxicity problems.[1]

Generally, the SHG process is not directly photodamaging the living environment because it is a scattering effect. However, at the laser wavelength, two-photon absorption and subsequent emission may occur so that excited state photochemistry could damage the sample. Thus, to avoid this, one must tune the molecular properties of such biotags.[2] A large first hyperpolarizability (β) is required for efficient SHG. Then, one can record the SHG signal of bright dyes with a low laser power, limiting photodamage. The exogenous biotags should also have a large β within the tissue transparency window (700−900 nm) and should involve minor one- and two-photon activities. Biotags such as fluorescent proteins can also be introduced by genetic engineering.

Some of us theoretically characterized the nonlinear optical (NLO) properties of fluorescent proteins at different theoretical levels of theory, including an ONIOM MP2:HF scheme where the first shell of residues around the chromophore was included in.[8−12] These investigations showed the importance to account for the H-bond network close to the chromophore and how the β of FPs strongly depends on the π-conjugation pathway, the degree of bond length alternation, and the presence of π-stacking interactions. Theoretical studies on compounds of interest for SHIM are still scarce.

In this contribution, we calculate and analyze the SHG response of small peptide chains and the peptide gramicidin A as models to understand the NLO properties of tryptophan-rich endogenous dyes. This is a follow-up work of the study of Duboisset et al.[13] who investigated experimentally the SHG response of an ensemble of tryptophan-rich peptides and gramicidin A. This set of systems is composed of KWK, KWWK, KWWWK, and KWWKWWK compounds where W and K denote tryptophan and lysine units, respectively. Gramicidin A is a natural peptide with the sequence VGALAVVVWLWLWLW, comprising four W units. Here, V, G, A, and L are the one-letter

Received: January 23, 2020
Revised: March 9, 2020
Published: March 9, 2020

https://dx.doi.org/10.1021/acs.jpcb.0c00643
J. Phys. Chem. B 2020, 124, 2568–2578

codes for the amino acids valine, glycine, alanine, and leucine, respectively. SHG signals were measured by hyper-Rayleigh scattering experiments at a wavelength of 784 nm, in Tris buffered aqueous solutions. While providing experimental reference first hyperpolarizabilities for this set of compounds, Duboisset et al.[13] showed that the β response follows an additive scheme with an increasing number of W units. It also appears that the first hyperpolarizability of a sole tryptophan strongly differs from a KWK one. They argued that the local environment created by both lysine units decreases its SHG response.

From a theoretical point of view, the first hyperpolarizability of these systems is difficult to evaluate not only because of their size but also because of conformational flexibility. This implies a large number of relevant structures at room temperature. Recently, two of us proposed the simplified time-dependent density functional theory (sTD-DFT) method[14] in its tight-binding (TB) version to evaluate the frequency-dependent first hyperpolarizability of large compounds with up to about 3000 atoms. With respect to a full TD-DFT treatment, the simplified method applies three approximations: (i) the exact Coulomb and exchange integrals are approximated by short-range damped Coulomb interactions of transition density monopoles, (ii) the CI excitation space is truncated as controlled by a single energy selection threshold parameter, and (iii) the response of the exchange−correlation functional is neglected.[15] For the evaluation of the first hyperpolarizability, two minor additional approximations are introduced, that is, both the Hartree exchange−correlation kernel and the third functional derivative of the exchange−correlation functional are neglected.[14] A semi-empirical tight-binding version called sTD-DFT-xTB also has been developed where instead of using KS-DFT input data, orbitals and eigenvalues from an extended basis set tight-binding calculation are employed.[16] It was shown that the sTD-DFT-xTB method can reproduce reasonably well β frequency dispersion of a collagen triple helix $[(\text{Pro-Pro-Gly})_{10}]_3$ and of fluorescent proteins with respect to ONIOM reference calculations.[14] Here, the sTD-DFT-xTB method is used to evaluate and understand dynamical structural effects on the SHG response for the set of tryptophan-rich short peptides and gramicidin A characterized experimentally by Duboisset et al.[13]

This article is organized as followed. First, we detail the calculations for this study and then present in the first results part, the analysis of the conformer ensembles for all systems with respect to their first hyperpolarizability properties. Structure−property relationships and the effect of sampling structures along a molecular dynamics (MD) trajectory is discussed. The last part of the Results section compares experimental first hyperpolarizabilities to computed values at different levels of theory. The Summary section concludes the main findings and possible implications of this work for future applications.

COMPUTATIONAL DETAILS

Figure 1 presents the structures of L-lysine (K) and L-tryptophan (W), which are the building blocks of all tryptophan-rich peptide compounds considered in this study. The secondary (rigid helical) structure of gramicidin A with highlighted tryptophan units is also shown. In order to evaluate the impact of conformational flexibility on the first hyperpolarizability as well as for determining the lowest energy conformers, we used the RMSD-based meta-dynamics approach recently proposed by Grimme,[17−19] except for gramicidin A. First, the standard, ground-state tight-binding GFN2-xTB[20] method is used for the generation of the conformer ensemble. Solvation effects for

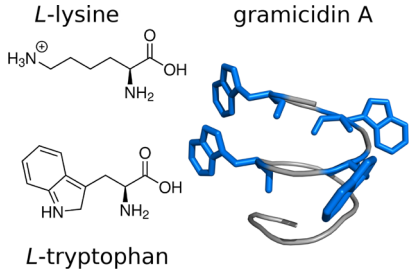

Figure 1. Lewis structures of amino acids lysine and tryptophan, building residues for the model peptides. Secondary structure of gramicidin A with blue highlighted tryptophan units.

water are implicitly accounted for using the GBSA[21,22] continuum model. Second, all conformers within a 6 kcal/mol GFN2-xTB energy window were optimized at the PBEh-3c(COSMO)[23,24] level of theory. Third, within a 4 kcal/mol PBEh-3c energy window all remaining structures were used as the input for PW6B95/def2-QZVP[25,26] single-point energy calculations. Free energies were computed for the lowest energy conformers by adding solvation free energies with COSMO-RS[27,28] and thermostatistical contributions within the modified[29] rigid-rotor harmonic oscillator approximation based on the GFN2-xTB computed Hessian ($\Delta G = \Delta E_{\text{PW6B95}} + \Delta G_{\text{solv}}^{\text{COSMO-RS}} + \Delta G_{\text{RRHO}}^{\text{GFN2-}x\text{TB}}$). The Boltzmann weights used correspond to a temperature of 298.15 K. The first hyperpolarizability of relevant conformers (population larger than 1.5%) were determined at the sTD-DFT-xTB/GBSA level of theory with modified Coulomb y_J and exchange y_K parameters set to 1.0 and 0.55, respectively. To further explore dynamic structural effects, MD simulations were carried out for 1 ns at the GFN2-xTB level of theory with preceding equilibration. In the simulations, a time step of 4 fs was used and the SHAKE[30,31] algorithm was applied, constraining all covalent bonds. The lowest conformer was used as the starting point for the MD simulations. From the resulting trajectory 200 snapshots were taken equidistantly and used as the structural input for the sTD-DFT-xTB/GBSA[14] calculations.

All sTD-DFT-xTB/GBSA calculations were performed with a configuration selection threshold of 10 eV. Note that the GBSA solvation model is only applied in the (ground state) orbitals generation step, meaning that non-equilibrium solvent effects on the first hyperpolarizability are not accounted for. These effects usually enhance the SHG response.[32−35] As already mentioned in the original publication of the method,[14] the underlying sTD-DFT-xTB parameterization—originally developed for excitation energies and absorption spectra—is not perfectly suited for NLO properties which more strongly depend on the high-energy part of the excitation manifold. We employ a small model system for benchmarking and adjustment purposes, that is, performing high-level calculations for reference β values and then to tune sTD-DFT-xTB Coulomb y_J and exchange y_K parameters accordingly. We computed the static β_{HRS} of tryptophan at the CCSD(T)/aug-cc-pVDZ[36] level of theory using the automatic finite-field (FF) Romberg differentiation procedure.[37] Its missing frequency dispersion was accounted for using the multiplicative approximation $\left(\beta_{\text{CC}}^{\omega} = \beta_{\text{CC}}^{0} \frac{\beta_{\text{TDHF or M06-2X}}^{\omega}}{\beta_{\text{TDHF or M06-2X}}^{0}}\right)$.

Figure 2 shows the adjusted sTD-DFT-xTB β_{HRS} curve matching, almost perfectly, the CCSD(T) one with the M06-2X frequency dispersion when using a y_J parameter of 1.0 instead of the original value of 4.0 and y_K of 0.55 instead of 2.0. For all

https://dx.doi.org/10.1021/acs.jpcb.0c00643
J. Phys. Chem. B 2020, 124, 2568−2578

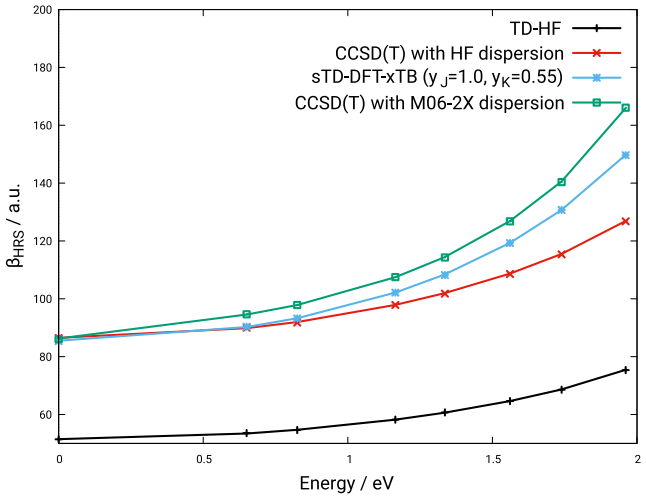

Figure 2. Frequency dispersion for tryptophan computed with CCSD(T)/aug-cc-pVDZ (red), TDHF/aug-cc-pVDZ (black), and sTD-DFT-*x*TB (blue) methods.

the following sTD-DFT-*x*TB calculations, the y_J and y_K parameters are set to 1.0 and 0.55, respectively.

Time-dependent Hartree−Fock (TDHF) calculations were also conducted for lowest energy conformers with the 6-31+G(d) basis set with and without solvent effects accounted for using the IEF-PCM scheme.[38,39] Note that when comparing TDHF results to the experiment, the static and dynamic dielectric constants of water differ largely. Thus, we selected a value at a large wavelength of 1900 nm instead of the static one. This wavelength is chosen to enable nonbiased comparisons and should be large enough to prevent any (near) resonance effects. For the smaller systems W and KWK, we also computed the response with the slightly larger aug-cc-pVDZ basis set showing very small differences with respect to 6-31+G(d) (see Tables S1 and S2). In the experimental work of Duboisset et al.,[13] the hyper-Rayleigh scattering value β_{HRS}[40] was measured. Theoretically, the following definition of β_{HRS} is used as the mean of β-tensor orientations

$$\beta_{HRS}(-2\omega;\,\omega,\,\omega) = \sqrt{\{\langle\beta_{ZZZ}^2\rangle + \langle\beta_{ZXX}^2\rangle\}} \tag{1}$$

where molecular averages without assuming Kleinman's conditions[41] are defined in the laboratory frame as

$$\begin{aligned}\langle\beta_{ZZZ}^2\rangle = {} & \frac{1}{7}\sum_{\zeta}^{x,y,z}\beta_{\zeta\zeta\zeta}^2 + \frac{4}{35}\sum_{\zeta\neq\eta}^{x,y,z}\beta_{\zeta\zeta\eta}^2 + \frac{2}{35}\sum_{\zeta\neq\eta}^{x,y,z}\beta_{\zeta\zeta\zeta}\beta_{\zeta\eta\eta} \\ & + \frac{4}{35}\sum_{\zeta\neq\eta}^{x,y,z}\beta_{\eta\zeta\zeta}\beta_{\zeta\zeta\eta} + \frac{4}{35}\sum_{\zeta\neq\eta}^{x,y,z}\beta_{\zeta\zeta\zeta}\beta_{\eta\eta\zeta} \\ & + \frac{1}{35}\sum_{\zeta\neq\eta}^{x,y,z}\beta_{\eta\zeta\zeta}^2 + \frac{4}{105}\sum_{\zeta\neq\eta\neq\xi}^{x,y,z}\beta_{\zeta\zeta\eta}\beta_{\eta\xi\xi} \\ & + \frac{1}{105}\sum_{\zeta\neq\eta\neq\xi}^{x,y,z}\beta_{\eta\zeta\zeta}\beta_{\eta\xi\xi} + \frac{4}{105}\sum_{\zeta\neq\eta\neq\xi}^{x,y,z}\beta_{\zeta\zeta\eta}\beta_{\xi\xi\eta} \\ & + \frac{2}{105}\sum_{\zeta\neq\eta\neq\xi}^{x,y,z}\beta_{\zeta\eta\xi}^2 + \frac{4}{105}\sum_{\zeta\neq\eta\neq\xi}^{x,y,z}\beta_{\zeta\eta\xi}\beta_{\eta\zeta\xi}\end{aligned} \tag{2}$$

and

$$\begin{aligned}\langle\beta_{ZXX}^2\rangle = {} & \frac{1}{35}\sum_{\zeta}^{x,y,z}\beta_{\zeta\zeta\zeta}^2 + \frac{4}{105}\sum_{\zeta\neq\eta}^{x,y,z}\beta_{\zeta\zeta\zeta}\beta_{\zeta\eta\eta} \\ & - \frac{2}{35}\sum_{\zeta\neq\eta}^{x,y,z}\beta_{\zeta\zeta\zeta}\beta_{\eta\eta\zeta} + \frac{8}{105}\sum_{\zeta\neq\eta}^{x,y,z}\beta_{\zeta\zeta\eta}^2 + \frac{3}{35}\sum_{\zeta\neq\eta}^{x,y,z}\beta_{\zeta\eta\eta}^2 \\ & - \frac{2}{35}\sum_{\zeta\neq\eta}^{x,y,z}\beta_{\zeta\zeta\eta}\beta_{\eta\zeta\zeta} + \frac{1}{35}\sum_{\zeta\neq\eta\neq\xi}^{x,y,z}\beta_{\zeta\eta\eta}\beta_{\zeta\xi\xi} \\ & - \frac{2}{105}\sum_{\zeta\neq\eta\neq\xi}^{x,y,z}\beta_{\zeta\zeta\xi}\beta_{\eta\eta\xi} - \frac{2}{105}\sum_{\zeta\neq\eta\neq\xi}^{x,y,z}\beta_{\zeta\zeta\eta}\beta_{\eta\xi\xi} \\ & + \frac{2}{35}\sum_{\zeta\neq\eta\neq\xi}^{x,y,z}\beta_{\zeta\eta\xi}^2 - \frac{2}{105}\sum_{\zeta\neq\eta\neq\xi}^{x,y,z}\beta_{\zeta\eta\xi}\beta_{\eta\zeta\xi}\end{aligned} \tag{3}$$

In addition from these quantities, the depolarization ratio can be obtained

$$DR = \frac{I_{VV}^{2\omega}}{I_{HV}^{2\omega}} = \frac{\langle\beta_{ZZZ}^2\rangle}{\langle\beta_{ZXX}^2\rangle} \tag{4}$$

where a value of 1.5 corresponds to a fully octupolar response, of 5 to a one-dimensional push−pull π-conjugated system, and of 9 to a fully dipolar system. Furthermore, it is useful to analyze the β tensor in terms of its dipolar ($J = 1$) and octupolar ($J = 3$) tensorial β_J-components[42]

$$\beta_{HRS} = \sqrt{\langle\beta_{HRS}^2\rangle} = \sqrt{\frac{10}{45}\,|\beta_{J=1}|^2 + \frac{10}{105}\,|\beta_{J=3}|^2} \tag{5}$$

where

$$\begin{aligned}|\beta_{J=1}|^2 = {} & \frac{3}{5}\sum_{\zeta}^{x,y,z}\beta_{\zeta\zeta\zeta}^2 + \frac{6}{5}\sum_{\zeta\neq\eta}^{x,y,z}\beta_{\zeta\zeta\zeta}\beta_{\zeta\eta\eta} + \frac{3}{5}\sum_{\zeta\neq\eta}^{x,y,z}\beta_{\eta\zeta\zeta}^2 \\ & + \frac{3}{5}\sum_{\zeta\neq\eta\neq\xi}^{x,y,z}\beta_{\eta\zeta\zeta}\beta_{\eta\xi\xi}\end{aligned} \tag{6}$$

$$\begin{aligned}|\beta_{J=3}|^2 = {} & \frac{2}{5}\sum_{\zeta}^{x,y,z}\beta_{\zeta\zeta\zeta}^2 - \frac{6}{5}\sum_{\zeta\neq\eta}^{x,y,z}\beta_{\zeta\zeta\zeta}\beta_{\zeta\eta\eta} + \frac{12}{5}\sum_{\zeta\neq\eta}^{x,y,z}\beta_{\eta\zeta\zeta}^2 \\ & - \frac{3}{5}\sum_{\zeta\neq\eta\neq\xi}^{x,y,z}\beta_{\eta\zeta\zeta}\beta_{\eta\xi\xi} + \sum_{\zeta\neq\eta\neq\xi}^{x,y,z}\beta_{\zeta\eta\xi}^2\end{aligned} \tag{7}$$

Using this decomposition, the electronic character of a NLO chromophore can be analyzed. We used a loss-less 3D visualization of the first hyperpolarizability tensor, to have a more intuitive analysis tool for the β tensor.[43] This so-called unit-sphere representation (USR) uses effective SHG dipoles, which are defined as

$$\vec{\beta}_{eff} = \overleftrightarrow{\beta} : \hat{E}(\theta,\,\phi)\hat{E}(\theta,\,\phi) \tag{8}$$

Taking all possible incident polarization directions defined by (θ,ϕ), a unit-sphere is mapped out (at a field value of $\hat{E}(\theta,\phi)$ 1 au). At these sampled points on the unit-sphere surface, the corresponding $\vec{\beta}_{eff}$ is plotted. This scheme allows a three-dimensional visualization of the β tensor without losing any information. Another approach for visualizing the β tensor, but at the cost of losing anisotropic information, consists of defining a vector, having the following components[44]

https://dx.doi.org/10.1021/acs.jpcb.0c00643
J. Phys. Chem. B 2020, 124, 2568−2578

$$\beta_x = \beta_{xxx} + \beta_{xyy} + \beta_{xzz}; \qquad \beta_y = \beta_{yxx} + \beta_{yyy} + \beta_{yzz};$$
$$\beta_z = \beta_{zxx} + \beta_{zyy} + \beta_{zzz} \tag{9}$$

All reported β values are given in atomic units [1 au of β = $3.6213\ 10^{-42}\ m^4\ V^{-1} = 3.2064\ 10^{-53}\ C^3\ m^3\ J^{-2} = 8.639\ 10^{-33}$ esu] within the Taylor series convention.[45] The CCSD(T) FF first hyperpolarizabilities were computed by the T-REX program natively interfaced with QChem version 5.1.[46] All TDHF calculations were carried out using the Gaussian 09 package.[47] For all DFT calculations TURBOMOLE version 7.2[48,49] was used with COSMOtherm version C3.0 release 1601[27,28] for COSMO-RS. The remaining calculations were conducted with the xtb[50] and stda[51] codes.

The first hyperpolarizability values of the tryptophan-rich peptides (β_{HRS}^{800}) were experimentally determined by Duboisset et al.[13] To eliminate the resonance effects and extrapolate to the static value,[52,53] we process the experimental data with the two-state approximation (TSA) proposed by Oudar and Chemla.[54]

$$F(\omega, \omega_{ge}, \gamma) = \frac{\beta_{zzz}(-2\omega, \omega, \omega)}{\beta_{zzz}(0,0,0)} = \frac{\omega_{ge}{}^2(\omega_{ge} - i\gamma)^2}{([\omega_{ge} - i\gamma]^2 - 4\omega^2)([\omega_{ge} - i\gamma]^2 - \omega^2)} \tag{10}$$

A homogeneous broadening of γ = 0.35 eV is applied while the experimental excitation energy of tryptophan ω_{ge} = 4.44 eV is used. Aside from the conventional TSA, inhomogeneous broadening or even the vibronic structure of the excited states could be accounted for.[6,52,53] However, using and comparing these refined extrapolation schemes for the studied systems goes beyond the scope of this study and would be inaccessible because some required experimental data are missing. Table 1 shows the dynamic and extrapolated experimental values.

RESULTS AND DISCUSSION

Conformers. Peptides in solution at ambient temperature are represented as a set of various conformers. Depending on the temperature, these are populated differently and the accessed conformational space can become quite large. The objective of this section is to analyze the conformational dependence of the SHG response, shedding light on this structure−property relationship. The above described theoretical multi-level approach provides a very reasonable conformational ensemble including solvation effects. For these sets of conformers, molecular first hyperpolarizabilities (static β_{HRS}) were computed. With the help of the described visualization techniques for the β tensor, the conformers of each system are compared in terms of their electronic and geometrical structures to show how they impact the NLO properties.

Table 1. Measured and Extrapolated (TSA) First Hyperpolarizabilites in Atomic Units

system	β_{HRS}^{800}	β_{HRS}^{∞}
W	544	240
KWK	100	44
KWWK	396	175
KWWWK	828	365
KWWKWWK	1215	536
gramicidin A	872	384

First, the tryptophan molecule is analyzed. For this system, the indole unit is essentially responsible for the first hyperpolarizability. Therefore, only small variations in β_{HRS} values are expected because of its rigid π-conjugated system. The amine and carboxylic acid moieties are flexible and the obtained conformer ensemble is mainly determined by their different orientations. Figure 3 shows the most contributing conformers at room temperature for tryptophan and their respective first hyperpolarizability values which do not differ much. The largest differences are caused by the re-orientation of the amine group. A small SHG enhancement is observed when local dipoles of the indole and amine units are perpendicular (conformer 2). This can be further visualized by the USR (see Figure S1). There, two conformers with the largest and smallest β_{HRS} values are shown (conformers 2 and 4). The pattern of effective SHG dipoles indicates a mix of dipolar and octupolar contributions. According to eq 5, for example, the $\beta_{HRS}{}^2$ value of conformer 2 contains 51% of dipolar and 49% of the octupolar contribution.

The second system is the model peptide KWK, a lysine capped tryptophan. The lysine groups were introduced for solubility reasons.[13] Experimentally, the observed difference in responses between tryptophan and KWK was attributed to the lysine side chains that shield the indole unit from the solvent. A large variety of conformers are found because of the high flexibility of these side chains. However, the rigid indole chromophore is unchanged among these conformers. Figure 4 presents the conformers and their first hyperpolarizability properties.

Note that sTD-DFT-*x*TB/GBSA calculations cannot account for nonequilibrium solvent effects on the response and hence part of the solvent-induced difference between tryptophan and KWK is missing. Thus, we conducted TDHF/IEF-PCM calculations for comparison that are discussed in the Supporting Information. Mostly, the picture emerging from the calculations is similar for both systems: several conformers of KWK are significantly populated, as for W. The USR for KWK (Figure S2) is more complex to analyze because of small dipolar contributions from both peptide bonds, but overall the response is similar to the one for W (i.e., a mix of dipolar and octupolar contributions). Note, however, that the relative $|\beta_{J=1}|$ and $|\beta_{J=3}|$ contributions to β_{HRS}^2 are quite different for, example, conformers 2 and 4 (with factors of 2.4 and 0.6 between the two contributions).

The third model peptide KWWK includes two chromophore units. The respective orientation of the two indole groups is mainly responsible for the change of the first hyperpolarizabilities among the ensemble. Figure 5 displays conformers of the KWWK model peptide, where the lysine groups and the peptide backbone are hidden to improve the visibility of chromophores.

Based on the results of tryptophan and KWK systems, we conclude that the effects of the saturated side chains are negligible for the SHG response. Therefore, the structure−property analysis is focused on the orientation of the indole moieties. For KWWK, the extreme β_{HRS} values differ by more than a factor of 2. The values among the ensemble show a larger spread than for the monochromophoric examples. The USR of both conformers—with the lowest (5) and highest (2) β_{HRS} values—shows that the orientation of the indole units plays an important role on the SHG response (see Figure 6). The indole units are aligned parallel in the second conformer with the largest first hyperpolarizability (232 au). On the other hand, one can observe a drastic decrease of the β_{HRS} value when the indole

https://dx.doi.org/10.1021/acs.jpcb.0c00643
J. Phys. Chem. B 2020, 124, 2568−2578

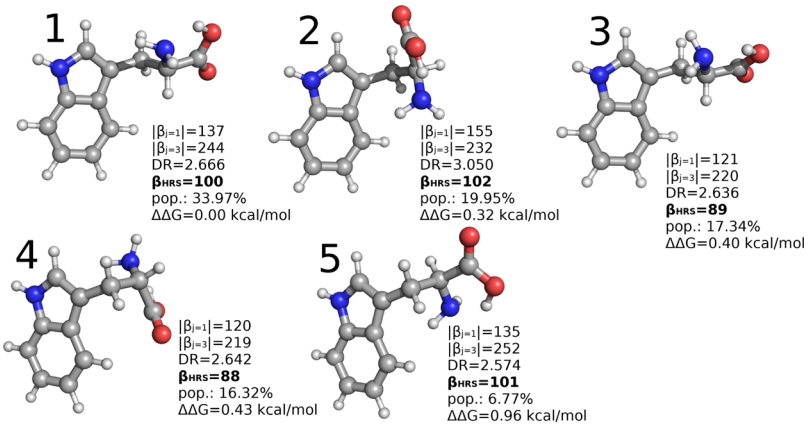

Figure 3. Conformer ensemble for tryptophan. First hyperpolarizability data ($|\beta_{J=1}|$, $|\beta_{J=3}|$, DR, β_{HRS}), population, and relative free energies are depicted with the plotted structures.

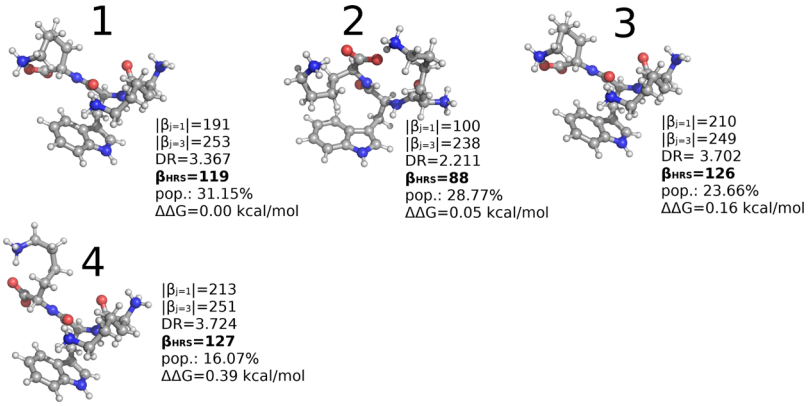

Figure 4. Conformer ensemble for model peptide KWK. First hyperpolarizability data ($|\beta_{J=1}|$, $|\beta_{J=3}|$, DR, β_{HRS}), population, and relative free energies are depicted with the plotted structures.

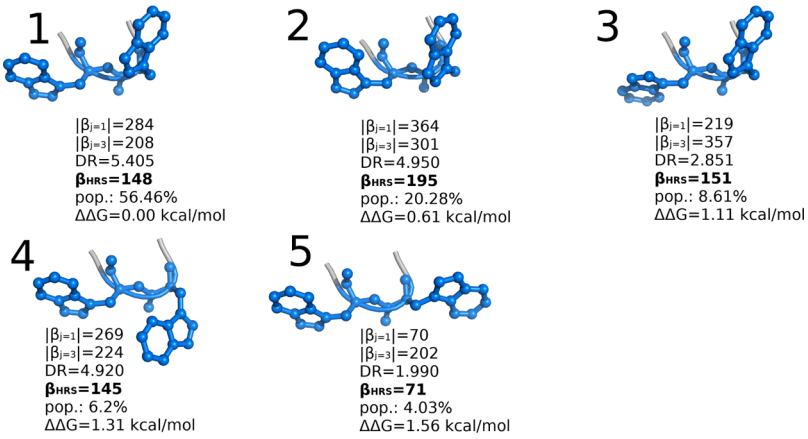

Figure 5. Conformer ensemble for model peptide KWWK. First hyperpolarizability data ($|\beta_{J=1}|$, $|\beta_{J=3}|$, DR, β_{HRS}), population, and relative free energies are depicted with the plotted structures.

units are antiparallel (71 au for conformer 5). The USR shows a very strong dipolar character of the β tensor, when the chromophore units are aligned parallel. In that case, the DR value of 4.95 confirms this. For opposite orientations, the octupolar component dominates the β tensor, as indicated by a DR value of 1.99.

For the larger KWWWK and KWWKWWK systems, similar observations as for KWWK are made. The orientation of the indole groups directly correlates with the magnitude of the first hyperpolarizability. The conformers of KWWWK and KWWKWWK are depicted in Figures 7 and 8, respectively. The two highest populated conformers of KWWWK differ by almost a factor of 1.5 in β_{HRS} values (1 and 2 with β_{HRS} = 181 au and 121 au, respectively). Conformer 1 has almost equal dipolar $|\beta_{J=1}|$ and octupolar $|\beta_{J=3}|$ values. Considering their weighting factors—10/45 and 10/105, respectively—a strong dipolar contribution to the β_{HRS} is observed, confirmed by a DR of 3.80. For this conformer, two indole units are more or less pointing in

https://dx.doi.org/10.1021/acs.jpcb.0c00643
J. Phys. Chem. B 2020, 124, 2568−2578

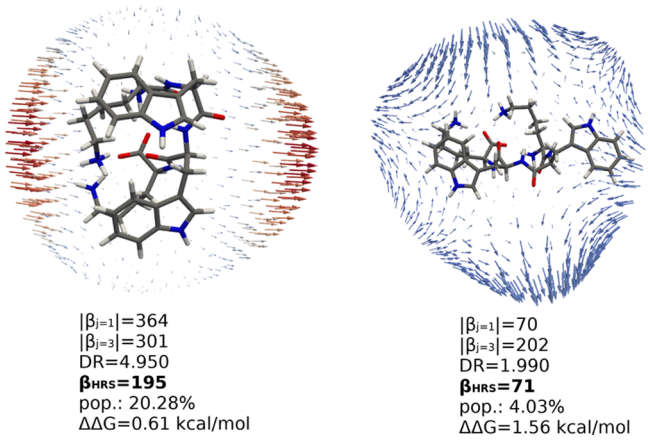

Figure 6. Unit-sphere representation for KWWK conformers 2 (left) and 5 (right). To increase visibility, the vector fields are differently scaled but arrow colors are consistent.

the same direction while one points in a different one (but not opposite). For conformer 2, this third indole unit changes its orientation to point in an opposite direction with respect to the first one, canceling each other. The dipolar contribution $|\beta_{J=1}|$ then equals only to 113 au, where the octupolar component is more than three times larger ($|\beta_{J=3}| = 349$ au). A DR value of 1.94 indicates an octupolar case for this conformer, which is corroborated by the USR depicted in Figure S3. This analysis shows that the inclusion of several conformers changes the β_{HRS} value compared to the one of the lowest energy conformers. In a later section, we will discuss whether this approach improves the first hyperpolarizability values in comparison to the experiment.

With four chromophore units, KWWKWWK is the largest example of all model peptides studied here. Figure 8 presents the six significantly populated conformer structures. Among this set, the conformers differ mostly by the orientation of their indole units. The first hyperpolarizability values spread by a factor of two between the conformers 3 and 4 (β_{HRS} = 234 and 112 au). For conformers 1, 3, and 6, the indole units are oriented roughly in the same manner, which is mainly due to the shared secondary structure. In the second group of trans-like conformers (2, 4 and 5), the indole units are partially oriented anti-parallel. This results in a decrease of the dipolar contribution to the β_{HRS}. The values for $|\beta_{J=1}|$ and $|\beta_{J=3}|$ indicate that for this cis-like group the dipolar contribution is dominant. The secondary structure can bend only because of the flexibility introduced by the third lysine unit. While the KWWWK ensemble is only dominated by a few conformers because of a rigid peptide backbone, the KWWKWWK ensemble is clearly enlarged by this added flexibility. For the interested reader, we provide in section S3, an analysis in terms of indole unit β vectors. They explain further the significant differences observed in the calculated SHG response among conformers.

Table 2 shows the first hyperpolarizability values for the lowest energy conformer and the Boltzmann-weighted ensemble. For tryptophan and KWK, the two values are very close to each other. As already described above, this is because of the rigidity of the chromophore. For the larger systems, we observed slightly larger differences between a single structure approach and the ensemble average. We explain this with the orientation of multiple chromophore units in ways that enhance or cancel the SHG response. The difference in β_{HRS} values (in au) between KWK and KWWK amounts to 30, to 32 for KWWK and KWWWK, and to 41 au for KWWWK and KWWKWWK. Because not all lowest energy conformers share the same indole orientation, these enhancements are not equal. When considering the Boltzmann weighted β_{HRS}, the differences can be quantified to 41, 13, and 35 au Also here, the enhancement is not perfectly linear. However, such a perfect linear enhancement is not realistic because the different conformers for the individual model peptides have a strong influence on the SHG response. These results clearly indicate that the addition of a tryptophan unit to these model peptides does not equally enhance the first hyperpolarizability.

Molecular Dynamics Sampling. In this section, we analyze the effect of using several structures from a MD simulation as the input for the evaluation of β. For the simulation of electronic circular dichroism spectra, some of us have already applied this approach successfully.[55−57] From a MD trajectory, snapshots are taken equidistantly and serve as input structures for the property calculations which are simply averaged over all included snapshots. In this process, no structural relaxations are included and the snapshots are equally weighted. By using a reasonably long simulation time, the considered structures should represent a Boltzmann ensemble.

Figure 9 shows the frequency dispersion of β for each snapshot as well as their average for the largest peptide KWWKWWK. The value of β_{HRS} changes drastically within a factor of six between the most extreme structures. This illustrates the sensitivity of this NLO property with respect to structural subtleties of a flexible system. However, when all snapshots are averaged, the resulting frequency dispersion of β_{HRS} does not

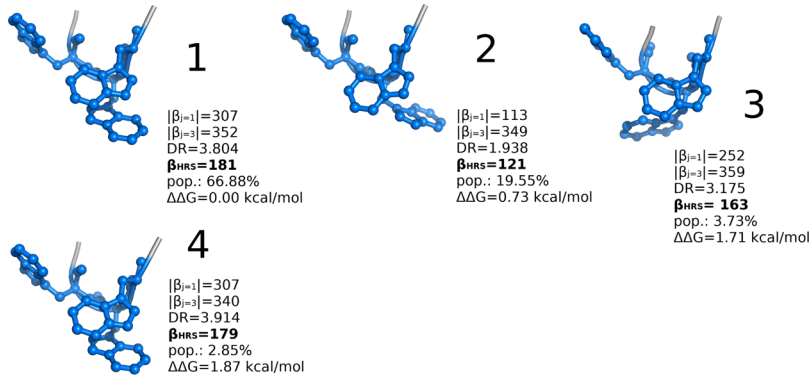

Figure 7. Conformer ensemble for model peptide KWWWK. First hyperpolarizability data ($|\beta_{J=1}|$, $|\beta_{J=3}|$, DR, β_{HRS}), population, and relative free energies are depicted with the plotted structures.

https://dx.doi.org/10.1021/acs.jpcb.0c00643
J. Phys. Chem. B 2020, 124, 2568−2578

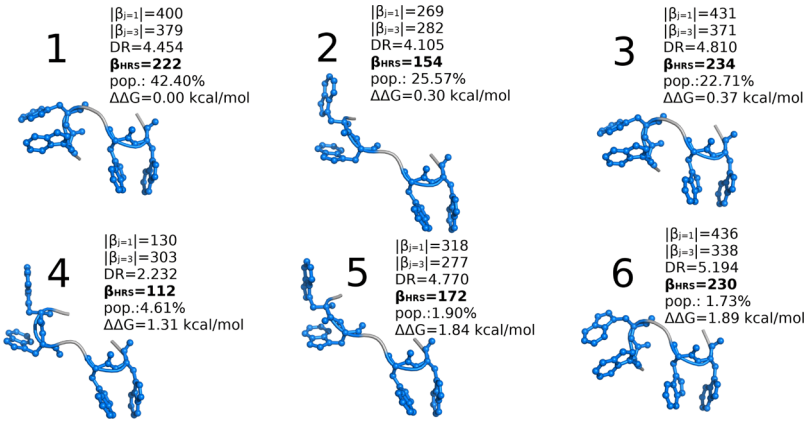

Figure 8. Conformer ensemble for model peptide KWWKWWK. First hyperpolarizability data ($|\beta_{J=1}|$, $|\beta_{J=3}|$, DR, β_{HRS}), population, and relative free energies are depicted with the plotted structures.

Table 2. Static First Hyperpolarizability Values (in au) for the Lowest Free Energy Conformer and the Boltzmann Weighted Ensemble Computed with sTD-DFT-*x*TB/GBSA

<!--Col Count:3-->system	minimum	ensemble
W	100	97
KWK	119	113
KWWK	149	154
KWWWK	181	167
KWWKWWK	222	202

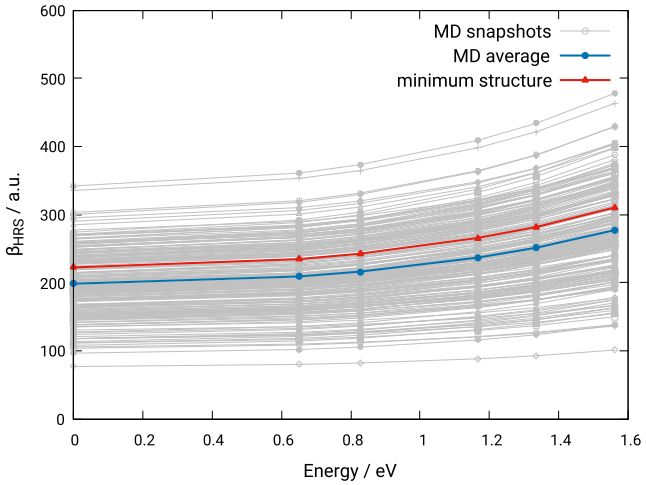

Figure 9. Frequency dispersion computed with sTD-DFT-*x*TB for 200 snapshots (gray), the MD average (blue), and for the optimized minimum structure (red) for the KWWKWWK peptide.

differ much from the one that considers only the lowest energy conformer with a reduction of around 2−22%. The frequency dispersion of the Boltzmann-weighted conformer ensemble does not differ much from the MD-averaged ensemble (cf. Figure S8). Figure 10 shows selected snapshots from the MD trajectory giving the lowest, the highest, and intermediate values for the first hyperpolarizability. Analyzing the structures in terms of indole orientations corroborates the findings from the previous section. When all indole units are oriented along the same direction, the largest β_{HRS} values are obtained. Considering the structure with the minimum response, we observe that two indole units are pointing in opposite directions, canceling out

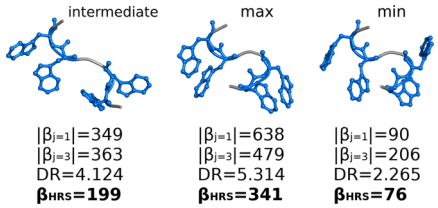

Figure 10. Selected MD structures for model peptide KWWKWWK. First hyperpolarizability data ($|\beta_{J=1}|$, $|\beta_{J=3}|$, DR and β_{HRS}) are depicted with the plotted structures.

their dipolar contributions to β, leaving a dominant octupolar character.

Table 3 shows MD-averaged static first hyperpolarizabilities for all model peptides. The difference in β_{HRS} values between the minimum structure (minimum) and MD-averaged structures (MD average) increases with the system size. This observation holds also for the difference between the minimum energy conformer and the conformer-weighted ensemble (ensemble). The first hyperpolarizability values of the ensemble differ from the ones of the MD average, except for the biggest system. Here, emphasize in the discussion on two systems. First, for tryptophan we obtain similar values for all three approaches. As already stated, this small difference is due to the negligible difference in the SHG response among the conformers. Second, for KWWKWWK, the small difference in the SHG response of ensemble and MD average can be assigned to a shallow PES. The energy difference between the first and the third most contributing conformers is only 0.35 kcal/mol and those conformers amount up to 91% of the entire population (see Figure 8). Thus, the MD simulation covers an ensemble that is comparable to the one from the equilibrium structure sampling

Table 3. Static First Hyperpolarizability Values for Lowest Energy Conformer (Minimum), Boltzmann-Weighted Ensemble (Ensemble), and Averaged MD Snapshots (MD Average) Computed with sTD-DFT-*x*TB/GBSA

system	minimum	ensemble	MD average
W	100	97	100
KWK	119	113	128
KWWK	149	154	142
KWWWK	181	167	152
KWWKWWK	222	202	198

https://dx.doi.org/10.1021/acs.jpcb.0c00643
J. Phys. Chem. B 2020, 124, 2568−2578

procedure. However, differences between the conformer-weighted ensemble and MD average are expected and present for the remaining systems because a simulation time of 1 ns is rather short to fully explore the conformational PES.

Comparison with Extrapolated Experimental Values. In this section, we compare the experimental values to the ones computed at the TDHF level with and without accounting for implicit solvation effects and at both sTD-DFT-*x*TB and sTD-DFT-*x*TB/GBSA levels. The frequency dispersion of β for all systems, computed with TDHF and sTD-DFT-*x*TB, is discussed in Section S5.

As geometries, we consider the lowest energy conformers for each system optimized with the PBEh-3c(COSMO) method. In the case of averaging all relevant conformers, the static β_{HRS} values were weighted by their respective Boltzmann weights. The static first hyperpolarizabilites (and at 1900 nm for TDHF/IEF-PCM results) are shown in Figure 11, which is divided in two panels: one for comparing tryptophan with KWK and one for every system except tryptophan.

First, we compare the β response of tryptophan and KWK. The experimental first hyperpolarizability values reveal a much weaker response (−80%) for KWK compared to tryptophan. This observation is only reproduced by the TDHF/IEF-PCM method, demonstrating the role of nonequilibrium solvent effects, though it yields only a difference of 20%. Because of the flexible side chains of KWK, the chromophore is partially shielded from the solvent. As speculated in the experimental paper, this could have a large effect on the electronic structure of the indole unit and thus also on the first hyperpolarizability. However, this hypothesis could not be corroborated by our calculations. The direct follow-up of this could be to investigate this effect by adding an explicit solvent shell. Second, the remaining systems are compared. The TDHF method without accounting for solvent effects is not able to reproduce the experimental trends. For a comparison of the frequency dispersion of TDHF and sTD-DFT-*x*TB see Figure S9. Applying an implicit solvation model improves the quality of the computed data. Except for gramicidin A, the experimental ordering is reproduced. The IEF-PCM scheme improves the β_{HRS} values with respect to the experiment. The sTD-DFT-*x*TB/GBSA method is also able to provide correct trends except for gramicidin A, but a systematic underestimation with respect to the experiment is observed, at least for the largest systems considered here. Note that the value obtained for the rigid gramicidin A is not so far from the experimental one. Including all relevant conformers has a small impact on the β_{HRS} values. The effect of weighting the conformers becomes more pronounced when changes between the indole subunit orientations become important. However, an accurate computation of free energies in solution for a proper Boltzmann weighting is difficult. Because the individual conformers largely differ in their β_{HRS} values, a slightly miscalculated population could lead directly to a bad result.

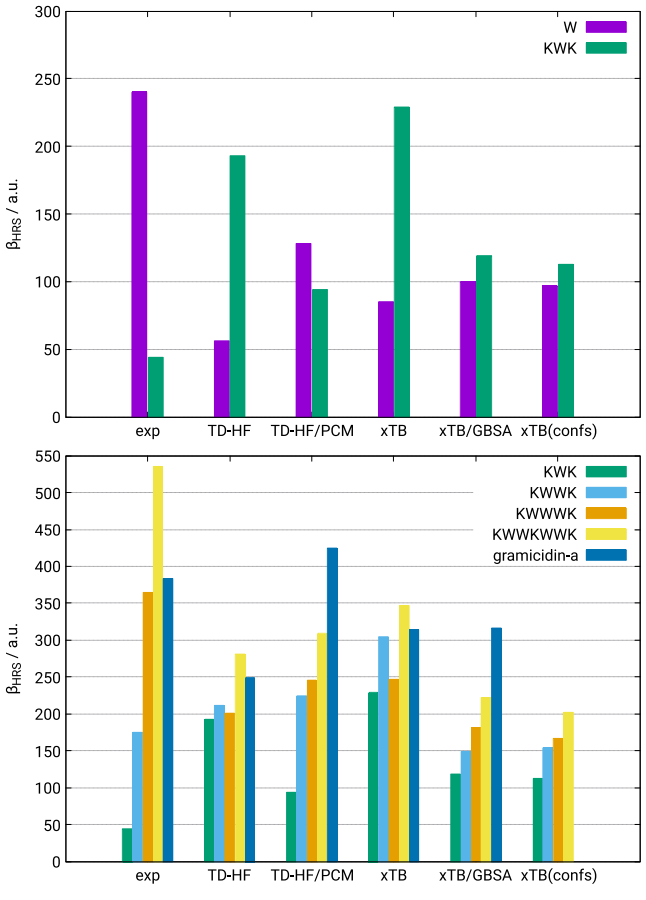

Figure 11. Static first hyperpolarizabilities for tryptophan and KWK (top) and KWK, KWWK, KWWWK, KWWKWWK, and gramicidin A (bottom) extrapolated from the experiment and computed with TDHF/6-31+G(d), TDHF/6-31+G(d)/PCM, sTD-DFT-*x*TB, sTD-DFT-*x*TB/GBSA, and Boltzmann-weighted ensemble with sTD-DFT-*x*TB/GBSA.

Table S5 shows the relative error for all methods. The relative mean absolute errors (MAEs, in au) of all methods are substantial, ranging from 0.94 (TDHF) to 0.46 (TDHF/IEF-PCM). The sTD-DFT-*x*TB/GBSA method provides a MAE of 0.62 very close to TDHF/IEF-PCM. It is especially remarkable considering that the sTD-DFT-*x*TB/GBSA calculations are 3−5 orders of magnitude faster than at the TDHF/IEF-PCM level of theory (see Table S3). Advances in including nonequilibrium solvent effects at the sTD-DFT-*x*TB/GBSA level could close this gap. For (s)TD-DFT, the paramount importance is already proved for calculations of first hyperpolarizabilities[32−35] and other properties.[58−60]

CONCLUSIONS

We have presented quantum chemical calculations and a structure−property analysis for NLO properties of tryptophan-rich model peptides. The sTD-DFT-*x*TB scheme enables computations for systems with up to several thousands of atoms and/or to screen large sets of structures. We used this method to sample the first hyperpolarizabilities with respect to structural changes for the flexible tryptophan-rich peptide chains. For this purpose, MD simulations as well as conformational sampling were carried out. This was done with the help of the efficient tight-binding-based method GFN2-*x*TB and a recently proposed approach for exploring the potential energy surface with meta-dynamics. To fine-tune the sTD-DFT-*x*TB scheme for the desired model peptides, two parameters were adjusted to reproduce CCSD(T) reference β values for tryptophan.

We first studied the conformer ensemble in terms of the relation between the relative orientations of indole moieties and the first hyperpolarizability. We found that a drastic change in β_{HRS} values relates to different alignments of indole dipoles among conformers. When they are aligned parallel, the value is enhanced while it diminishes when the dipole moments are pointing in opposite directions leading to first hyperpolariz-

https://dx.doi.org/10.1021/acs.jpcb.0c00643
J. Phys. Chem. B 2020, 124, 2568−2578

ability values of conformers that can differ by a factor of up to two. This highlights the importance of finding the lowest energy conformer when calculating the SHG response. The unit-sphere representations clearly showed, in most of the cases, the dipolar character of the β tensor. The assumption that the sum of indole dipole vectors is correlated to the intensity of the first hyperpolarizability was confirmed by model system calculations. The results of the MD simulations indicate, additionally, a very strong sensitivity of the first hyperpolarizability to details of the molecular structure. Overall it seems essential to properly explore the conformational space of flexible chromophores or when multiple chromophore orientations are possible.

In the second part, we compared sTD-DFT-*x*TB computed first hyperpolarizabilities to the TDHF values and to the experiment. sTD-DFT-*x*TB and TDHF perform similarly in terms of reproducing the experimental trend of the SHG response. Cases where the methods produce incorrect order of values with respect to the size of the system were found at both levels of theories. This is mostly when solvent effects are not included. The sTD-DFT-*x*TB method is able to provide SHG response values for tryptophan-rich systems at a fraction of the cost of the usually used TDHF level of theory. The comparison of theoretical with experimental values shows that getting a quantitative agreement is a challenging task. TDHF/IEF-PCM performs slightly better than sTD-DFT-*x*TB/GBSA probably due to the inclusion of additional nonequilibrium solvent effects. The sTD-DFT-*x*TB scheme can be routinely applied to systems that are inaccessible with TDHF, while still expecting reasonable accuracy. Considering this efficiency, a future study could investigate how the relation between the first hyperpolarizability and the number of tryptophan units evolve for larger peptides. This relation is not expected to be linear because of the sensitivity of the property on indole unit orientations. Another area of future research is the impact of an explicit solvation on the conformational ensembles and their SHG response.

■ ASSOCIATED CONTENT

Supporting Information

The Supporting Information is available free of charge at https://pubs.acs.org/doi/10.1021/acs.jpcb.0c00643.

(PDF)

■ AUTHOR INFORMATION

Corresponding Authors

Stefan Grimme − *Mulliken Center for Theoretical Chemistry, Institut für Physikalische und Theoretische Chemie der Universität Bonn, D-53115 Bonn, Germany;* orcid.org/0000-0002-5844-4371; Phone: +49 228 73 2544; Email: grimme@thch.uni-bonn.de

Marc de Wergifosse − *Mulliken Center for Theoretical Chemistry, Institut für Physikalische und Theoretische Chemie der Universität Bonn, D-53115 Bonn, Germany;* orcid.org/0000-0002-9564-7303; Phone: +49 228 73 60432; Email: mdewergifosse@gmail.com

Authors

Jakob Seibert − *Mulliken Center for Theoretical Chemistry, Institut für Physikalische und Theoretische Chemie der Universität Bonn, D-53115 Bonn, Germany;* orcid.org/0000-0002-3163-8627

Benoît Champagne − *Laboratoire de Chimie Théorique, Université de Namur, B-5000 Namur, Belgium;* orcid.org/0000-0003-3678-8875

Complete contact information is available at: https://pubs.acs.org/10.1021/acs.jpcb.0c00643

Notes

The authors declare no competing financial interest.

■ ACKNOWLEDGMENTS

This work was supported by the DFG in the framework of the Gottfried-Wilhelm-Leibniz prize.

■ REFERENCES

(1) Campagnola, P. J.; Loew, L. M. Second-harmonic imaging microscopy for visualizing biomolecular arrays in cells, tissues and organisms. *Nat. Biotechnol.* **2003**, *21*, 1356−1360.

(2) Reeve, J. E.; Anderson, H. L.; Clays, K. Dyes for biological second harmonic generation imaging. *Phys. Chem. Chem. Phys.* **2010**, *12*, 13484−13498.

(3) Campagnola, P. Second harmonic generation imaging microscopy: Applications to diseases diagnostics. *Anal. Chem.* **2011**, *83*, 3224−3231.

(4) Pavone, F. S.; Campagnola, P. J. *Second Harmonic Generation Imaging*; CRC Press, 2013.

(5) Deniset-Besseau, A.; Duboisset, J.; Benichou, E.; Hache, F.; Brevet, P.-F.; Schanne-Klein, M.-C. Measurement of the second-order hyperpolarizability of the collagen triple helix and determination of its physical origin. *J. Phys. Chem. B* **2009**, *113*, 13437−13445.

(6) de Wergifosse, M.; De Ruyck, J.; Champagne, B. How the second-order nonlinear optical response of the collagen triple helix appears: A theoretical investigation. *J. Phys. Chem. C* **2014**, *118*, 8595−8602.

(7) Harczuk, I.; Vahtras, O.; Ågren, H. First hyperpolarizability of collagen using the point dipole approximation. *J. Phys. Chem. Lett.* **2016**, *7*, 2132−2138.

(8) De Meulenaere, E.; Asselberghs, I.; de Wergifosse, M.; Botek, E.; Spaepen, S.; Champagne, B.; Vanderleyden, J.; Clays, K. Second-order nonlinear optical properties of fluorescent proteins for second-harmonic imaging. *J. Mater. Chem.* **2009**, *19*, 7514−7519.

(9) De Meulenaere, E.; de Wergifosse, M.; Botek, E.; Spaepen, S.; Champagne, B.; Vanderleyden, J.; Clays, K. Nonlinear optical properties of mStrawberry and mCherry for second harmonic imaging. *J. Nonlinear Opt. Phys. Mater.* **2010**, *19*, 1−13.

(10) De Meulenaere, E.; de Wergifosse, M.; Botek, E.; Vanderleyden, J.; Champagne, B.; Clays, K. Prediction of first hyperpolarizability of fluorescent proteins. *AIP Conf. Proc.* **2015**, *1642*, 522−525.

(11) De Meulenaere, E.; Nguyen Bich, N.; de Wergifosse, M.; Van Hecke, K.; Van Meervelt, L.; Vanderleyden, J.; Champagne, B.; Clays, K. Improving the second-order nonlinear optical response of fluorescent proteins: The symmetry argument. *J. Am. Chem. Soc.* **2013**, *135*, 4061−4069.

(12) de Wergifosse, M.; Botek, E.; De Meulenaere, E.; Clays, K.; Champagne, B. ONIOM Investigation of the second-order nonlinear optical responses of fluorescent proteins. *J. Phys. Chem. B* **2018**, *122*, 4993−5005.

(13) Duboisset, J.; Matar, G.; Besson, F.; Ficheux, D.; Benichou, E.; Russier-Antoine, I.; Jonin, C.; Brevet, P. F. Second harmonic generation from tryptophan-rich short peptides: WNKM and gramicidin A. *J. Phys. Chem. B* **2014**, *118*, 10413−10418.

(14) de Wergifosse, M.; Grimme, S. Nonlinear-response properties in a simplified time-dependent density functional theory (sTD-DFT) framework: Evaluation of the first hyperpolarizability. *J. Chem. Phys.* **2018**, *149*, 024108.

(15) Grimme, S. A simplified Tamm-Dancoff density functional approach for the electronic excitation spectra of very large molecules. *J. Chem. Phys.* **2013**, *138*, 244104.

(16) Grimme, S.; Bannwarth, C. Ultra-fast computation of electronic spectra for large systems by tight-binding based simplified Tamm-Dancoff approximation (sTDA-xTB). *J. Chem. Phys.* **2016**, *145*, 054103.
(17) Grimme, S. Exploration of chemical compound, conformer, and reaction space with meta-dynamics simulations based on tight-binding quantum chemical calculations. *J. Chem. Theory Comput.* **2019**, *15*, 2847−2862.
(18) Grimme, S.; Bannwarth, C.; Dohm, S.; Hansen, A.; Pisarek, J.; Pracht, P.; Seibert, J.; Neese, F. Fully automated quantum-chemistry-based computation of spin-spin-coupled nuclear magnetic resonance spectra. *Angew. Chem., Int. Ed.* **2017**, *56*, 14763−14769.
(19) Pracht, P.; Bohle, F.; Grimme, S. Automated exploration of the low-energy chemical space with fast quantum chemical methods. *Phys. Chem. Chem. Phys.* **2020**, DOI: 10.1039/C9CP06869D, in press.
(20) Bannwarth, C.; Ehlert, S.; Grimme, S. GFN2-xTB - an accurate and broadly parametrized self-consistent tight-binding quantum chemical method with multipole electrostatics and density-dependent dispersion contributions. *J. Chem. Theory Comput.* **2018**, *15*, 1652−1671.
(21) Grimme, S.; Bannwarth, C.; Shushkov, P. A robust and accurate tight-binding quantum chemical method for structures, vibrational frequencies, and noncovalent interactions of large molecular systems parametrized for all spd-block elements (Z = 1−86). *J. Chem. Theory Comput.* **2017**, *13*, 1989−2009.
(22) Still, W. C.; Tempczyk, A.; Hawley, R. C.; Hendrickson, T. Semianalytical treatment of solvation for molecular mechanics and dynamics. *J. Am. Chem. Soc.* **1990**, *112*, 6127−6129.
(23) Grimme, S.; Brandenburg, J. G.; Bannwarth, C.; Hansen, A. Consistent structures and interactions by density functional theory with small atomic orbital basis sets. *J. Chem. Phys.* **2015**, *143*, 054107.
(24) Klamt, A.; Schüürmann, G. COSMO: a new approach to dielectric screening in solvents with explicit expressions for the screening energy and its gradient. *J. Chem. Soc., Perkin Trans. 2* **1993**, 799−805.
(25) Zhao, Y.; Truhlar, D. G. Design of density functionals that are broadly accurate for thermochemistry, thermochemical kinetics, and nonbonded interactions. *J. Phys. Chem. A* **2005**, *109*, 5656−5667.
(26) Weigend, F.; Ahlrichs, R. Balanced basis sets of split valence, triple zeta valence and quadruple zeta valence quality for H to Rn: Design and assessment of accuracy. *Phys. Chem. Chem. Phys.* **2005**, *7*, 3297−3305.
(27) Eckert, F.; Klamt, A. Fast solvent screening via quantum chemistry: COSMO-RS approach. *AIChE J.* **2002**, *48*, 369−385.
(28) *COSMOtherm*, C3.0, release 1601, COSMOlogic GmbH & Co KG, http://www.cosmologic.de.
(29) Grimme, S. Supramolecular binding thermodynamics by dispersion-corrected density functional theory. *Chem. - Eur. J.* **2012**, *18*, 9955−9964.
(30) Ryckaert, J.-P.; Ciccotti, G.; Berendsen, H. J. C. Numerical integration of the cartesian equations of motion of a system with constraints: molecular dynamics of n-alkanes. *J. Comput. Phys.* **1977**, *23*, 327−341.
(31) van Gunsteren, W. F.; Berendsen, H. J. C. Algorithms for macromolecular dynamics and constraint dynamics. *Mol. Phys.* **1977**, *34*, 1311−1327.
(32) Yu, J.; Zerner, M. C. Solvent effect on the first hyperpolarizabilities of conjugated organic molecules. *J. Chem. Phys.* **1994**, *100*, 7487−7494.
(33) Zhu, W.; Wu, G.-S. An ab initio study of the first hyperpolarizabilities of octupolar substituted triazines: Electron correlation, solvent effect and frequency dispersion. *Chem. Phys. Lett.* **2002**, *358*, 1−7.
(34) Yamaguchi, Y.; Yokomichi, Y.; Yokoyama, S.; Mashiko, S. Theoretical study of solvent effects of first-order hyperpolarizabilities of nitro-azobenzene dendrimers. *J. Mol. Struct.: THEOCHEM* **2002**, *578*, 35−45.
(35) Cammi, R.; Cossi, M.; Mennucci, B.; Tomasi, J. Solvent effects on static and dynamic polarizability and hyperpolarizabilities of acetonitrile. *J. Mol. Struct.* **1997**, *436−437*, 567−575.
(36) Dunning, T. H. Gaussian basis sets for use in correlated molecular calculations. I. The atoms boron through neon and hydrogen. *J. Chem. Phys.* **1989**, *90*, 1007−1023.
(37) de Wergifosse, M.; Liégeois, V.; Champagne, B. Evaluation of the molecular static and dynamic first hyperpolarizabilities. *Int. J. Quantum Chem.* **2014**, *114*, 900−910.
(38) Cancès, E.; Mennucci, B.; Tomasi, J. A new integral equation formalism for the polarizable continuum model: Theoretical background and applications to Isotropic and anisotropic dielectrics. *J. Chem. Phys.* **1997**, *107*, 3032−3041.
(39) Cancès, E.; Mennucci, B. Comment on "reaction field treatment of charge penetration" [J. Chem. Phys. 112, 5558 (2000)]. *J. Chem. Phys.* **2001**, *114*, 4744−4745.
(40) Verbiest, T.; Clays, K.; Rodriguez, V. *Second-Order Nonlinear Optical Characterization Techniques: an Introduction*; CRC press, 2009.
(41) Bersohn, R.; Pao, Y.-H.; Frisch, H. L. Double-quantum light scattering by molecules. *J. Chem. Phys.* **1966**, *45*, 3184−3198.
(42) Castet, F.; Bogdan, E.; Plaquet, A.; Ducasse, L.; Champagne, B.; Rodriguez, V. Reference molecules for nonlinear optics: A joint experimental and theoretical investigation. *J. Chem. Phys.* **2012**, *136*, 024506.
(43) Tuer, A.; Krouglov, S.; Cisek, R.; Tokarz, D.; Barzda, V. Three-dimensional visualization of the first hyperpolarizability tensor. *J. Comput. Chem.* **2011**, *32*, 1128−1134.
(44) Guthmuller, J.; Simon, D. Linear and nonlinear optical response of aromatic amino acids: A time-dependent density functional investigation. *J. Phys. Chem. A* **2006**, *110*, 9967−9973.
(45) Willetts, A.; Rice, J. E.; Burland, D. M.; Shelton, D. P. Problems in the comparison of theoretical and experimental hyperpolarizabilities. *J. Chem. Phys.* **1992**, *97*, 7590−7599.
(46) Shao, Y.; et al. Advances in molecular quantum chemistry contained in the Q-Chem 4 program package. *Mol. Phys.* **2015**, *113*, 184−215.
(47) Frisch, M. J.; et al. *Gaussian 09*, 2009.
(48) Furche, F.; Ahlrichs, R.; Hättig, C.; Klopper, W.; Sierka, M.; Weigend, F. Turbomole. *Wiley Interdiscip. Rev.: Comput. Mol. Sci.* **2014**, *4*, 91−100.
(49) Ahlrichs, R.; Bär, M.; Häser, M.; Horn, H.; Kölmel, C. Electronic structure calculations on workstation computers: The program system turbomole. *Chem. Phys. Lett.* **1989**, *162*, 165−169.
(50) xtb Github page. https://github.com/grimme-lab/xtb (accessed December 2019).
(51) stda Github page. https://github.com/grimme-lab/stda (accessed December 2019).
(52) Campo, J.; Wenseleers, W.; Goovaerts, E.; Szablewski, M.; Cross, G. H. Accurate determination and modeling of the dispersion of the first hyperpolarizability of an efficient zwitterionic nonlinear optical chromophore by tunable wavelength hyper-rayleigh scattering. *J. Phys. Chem. C* **2008**, *112*, 287−296.
(53) Mançois, F.; Pozzo, J.-L.; Pan, J.; Adamietz, F.; Rodriguez, V.; Ducasse, L.; Castet, F.; Plaquet, A.; Champagne, B. Two-way molecular switches with large nonlinear optical contrast. *Chem.—Eur. J.* **2009**, *15*, 2560−2571.
(54) Oudar, J. L.; Chemla, D. S. Hyperpolarizabilities of the nitroanilines and their relations to the excited state dipole moment. *J. Chem. Phys.* **1977**, *66*, 2664−2668.
(55) Bannwarth, C.; Seibert, J.; Grimme, S. The electronic circular dichroism of [16] helicene with simplified TD-DFT: Beyond the single structure approach. *Chirality* **2016**, *28*, 365−369.
(56) Seibert, J.; Bannwarth, C.; Grimme, S. Biomolecular structure information from high-speed quantum mechanical electronic spectra calculation. *J. Am. Chem. Soc.* **2017**, *139*, 11682−11685.
(57) Seibert, J.; Pisarek, J.; Schmitz, S.; Bannwarth, C.; Grimme, S. Extension of the element parameter set for ultra-fast excitation spectra calculation (sTDA-xTB). *Mol. Phys.* **2019**, *117*, 1104−1116.

https://dx.doi.org/10.1021/acs.jpcb.0c00643
J. Phys. Chem. B 2020, 124, 2568−2578

(58) Caricato, M. A corrected-linear response formalism for the calculation of electronic excitation energies of solvated molecules with the CCSD-PCM method. *Comput. Theor. Chem.* **2014**, *1040−1041*, 99−105.
(59) Improta, R.; Scalmani, G.; Frisch, M. J.; Barone, V. Toward effective and reliable fluorescence energies in solution by a new state specific polarizable continuum model time dependent density functional theory approach. *J. Chem. Phys.* **2007**, *127*, 074504.
(60) Ponce-Vargas, M.; Azarias, C.; Jacquemin, D.; Le Guennic, B. Combined TD-DFT-SOS-CIS(D) study of BOPHY derivatives with potential application in biosensing. *J. Phys. Chem. B* **2017**, *121*, 10850−10858.

https://dx.doi.org/10.1021/acs.jpcb.0c00643
J. Phys. Chem. B 2020, 124, 2568−2578